BIOCHEMISTRY
including biophysical chemistry & molecular biology
Article

Biochemistry **2010,** *49,* 3887–3897 3887
DOI: 10.1021/bi902057a

Elimination of the Native Structure and Solubility of the hVAPB MSP Domain by the Pro56Ser Mutation That Causes Amyotrophic Lateral Sclerosis[†]

Jiahai Shi,[‡,∥] Shixiong Lua,[‡,∥] Justina Shihui Tong,[‡] and Jianxing Song*[,‡,§]

[‡]*Department of Biological Sciences, Faculty of Science, National University of Singapore, Singapore, and* [§]*Department of Biochemistry, Yong Loo Lin School of Medicine, National University of Singapore, 10 Kent Ridge Crescent, Singapore 119260* [∥]*These authors contributed equally to this work.*

Received December 2, 2009; Revised Manuscript Received April 2, 2010

ABSTRACT: The Pro56Ser mutation in the human VAPB MSP domain causes a familial amyotrophic lateral sclerosis. Here we present the first structural investigation of both wild-type and Pro56Ser mutant MSP domains. The results reveal that the wild-type MSP domain is well-folded at neutral pH but can undergo acid-induced unfolding reversibly. It has a thermodynamic stability energy ($\Delta G°_{N-U}$) of 7.40 kcal/mol and is also active in binding to a Nir2 peptide with a K_D of 0.65 μM. Further determination of its crystal structure reveals that it adopts a seven-strand immunoglobulin-like β sandwich in which Pro56 adopts the unusual cis-peptide bond conformation that appears to be critical in maintaining the characteristic S-shaped loop. Markedly, the Pro56Ser mutation renders the MSP domain insoluble in buffer. Nevertheless, as facilitated by our recent discovery that "insoluble proteins" can be solubilized in salt-free water, we have successfully characterized the residue-specific conformation of the Pro56Ser mutant by CD and heteronuclear NMR spectroscopy. The Pro56Ser mutant remains lacking of the native tight packing and secondary structures under various conditions and was further characterized as having a non-native helical conformation weakly populated at pH 3.5. Intriguingly, Pro12 located in another S-shaped loop also adopts the cis-peptide bond conformation, and its mutation to Ser is able to make the MSP domain highly insoluble and unfolded like the Pro56Ser mutant. Our study thus implies that the Pro56Ser mutation might lead to ALS by eliminating the native MSP structure, which consequently leads to aggregation and loss of functions under physiological conditions.

Amyotrophic lateral sclerosis (ALS, also known as Lou Gehrig's disease and motor neuron disease) is the most prevalent fatal motor neuron disease, characteristic of progressive loss of both upper and lower motor neurons. ALS affects people of all races and ethnic backgrounds; approximately 10% of the cases have hereditary background, while the rest are sporadic. So far, the exact mechanism underlying ALS has not been defined well, and there is no primary therapy for ALS. Since sporadic and familial ALS affects the same neurons with similar pathology, it is thought that knowledge and therapeutic approaches and agents developed on mutant models can be translated to sporadic ALS (*1*, *2*).

Four ALS-causative genes have been identified. The most characterized ALS1 encodes mutants of Cu/Zn-superoxide dismutase (SOD1), whose expression leads to neuronal cell death in vitro and an ALS-like phenotype in vivo. ALS2 encodes alsin protein which may exert a neuroprotective function, and its ablation caused mild motor disorder. ALS4 was recently identified and predicted to encode a DNA/RNA helicase with unknown function. Most recently, ALS8 at 20q13.3 was identified from a large Brazilian family with autosomal dominant motor neuron diseases, which encodes a mutated VAPB (vesicle-associated membrane protein-associated protein B). The missense P56S point mutation in VAPB results in a typical ALS phenotype with rapid progression or late onset spinal muscular atrophy (*2*−*5*).

[†]This study is supported by Ministry of Education (MOE) of Singapore Tier 2 Grant R-154-000-388-112 to J. Song.

*To whom correspondence should be addressed. Phone: 65 65161013. Fax: 65 6779 2486. E-mail: bchsj@nus.edu.sg.

The human VAP family proteins were initially identified as homologues of vesicle-associated membrane protein (VAMP)-associated protein (VAP) with a size of 33 kDa in *Aplysia californica* (aVAP33) (*6*, *7*), including VAPA, VAPB, and VAPC. VAPA and VAPB are ~60% identical in sequence, while VAPB and VAPC are alternatively spliced variants. VAP proteins are ubiquitously expressed, type II integral membrane proteins that localize to the endoplasmic reticulum (ER) and pre-Golgi intermediates (*8*), which have been implicated in the regulation of neurotransmitter release, ER−Golgi transport, and intra-Golgi transport (*9*, *10*). Moreover, VAP proteins have been shown to target lipid-binding proteins carrying a short motif containing two phenylalanines in an acidic tract (FFAT motif) to the ER (*11*, *12*). The FFAT motif consists of the consensus amino acid sequence EFFDAxE, which was conserved in several lipid-binding protein families implicated in the transfer of lipids between the ER and other organelles, such as the Golgi, endosomes, and plasma membrane (*13*−*17*). The VAP proteins also interact with intracellular proteins (*18*, *19*), including Nir1, Nir2, and Nir3 via the FFAT motif which differentially affects the organization of the ER (*10*). Most recently, it was also shown that the VAPB MSP domain was released by cleavage to serve as a ligand for Eph receptors (*20*).

Despite having very diverse functions, VAP proteins are composed of three conserved domains, namely, an N-terminal immunoglobulin-like β sheet domain that is 22% identical in sequence to the major sperm protein (MSP), a central coiled-coil domain, and a C-terminal transmembrane domain (Figure 1a). Previously, VAPB had been relatively less investigated than VAPA. However,

Published on Web 04/08/2010

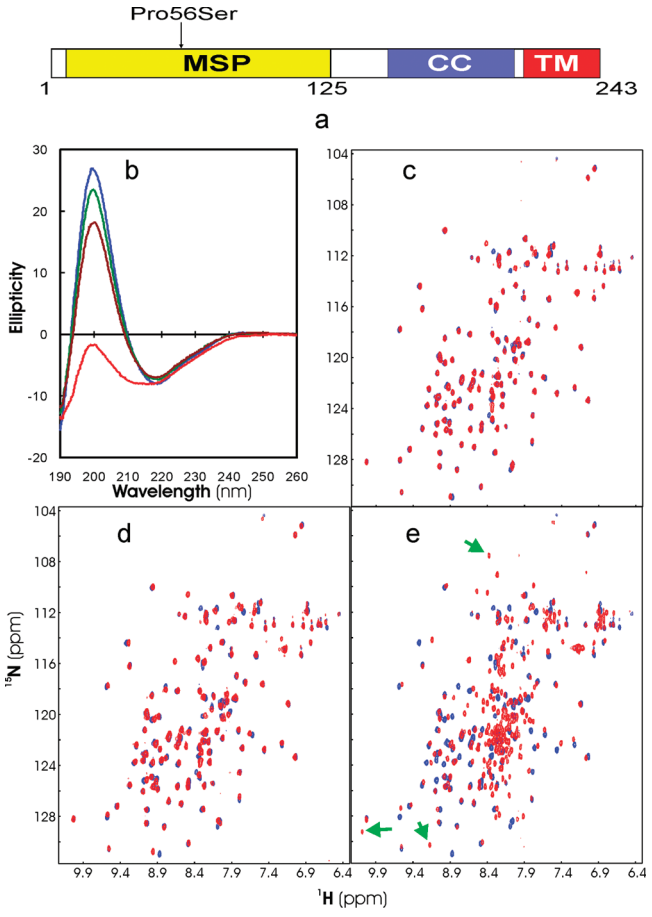

FIGURE 1: Structural characterization of the wild-type MSP domain. (a) Domain organization of the hVAPB protein that contains major sperm protein homology (MSP), coiled-coil (CC), and transmembrane (TM) domains. (b) Far-UV CD spectra of the wild-type MSP domain at a protein concentration of ~20 μM at pH 6.5 (blue), 5.5 (green), 4.5 (brown), and 3.5 (red). (c) Superimposition of the two-dimensional ^{1}H−^{15}N NMR HSQC spectra at a protein concentration of ~50 μM at pH 6.5 (blue) and 5.5 (red). (d) Superimposition of the HSQC spectra at pH 6.5 (blue) and 4.5 (red). (e) Superimposition of the HSQC spectra at pH 6.5 (blue) and 3.5 (red). Green arrows are used to indicate some HSQC peaks newly manifested at pH 3.5.

immediately after the Pro56Ser mutation of VAPB was associated with ALS, several studies have been reported on its functions and the biological consequence of the Pro56Ser mutation (*21*−*28*). Of particular interest is the implication of VAP proteins in mediating unfolded protein response (UPR) in the ER (*25*−*28*). Moreover, severe aggregation was observed on the Pro56Ser mutant, which has been proposed to play a pivotal role in the pathomechanism of ALS.

To fully understand the molecular mechanism underlying the VAPB mutation causing ALS, one essential step is to structurally characterize the wild-type VAPB MSP domain, followed by the assessment of the consequence of the Pro56Ser mutation. In this study, for the first time, we have determined the thermodynamic stability, activity, and crystal structure of the wild-type human VAPB (hVAPB) MSP domain. Most importantly, despite its insolubility in high-dielectric constant solutions, we have succeeded in determining residue-specific conformational properties of the Pro56Ser mutant by heteronuclear NMR spectroscopy, as facilitated by our recent discovery that previously thought insoluble proteins can in fact be solubilized in salt-free water (*29*−*33*). These results together not only provide a structural rationale for how the Pro56Ser mutation may lead to ALS but also imply a general mechanism by which the mutation or posttranslational modification causes aggregation of disease-related proteins in vivo.

EXPERIMENTAL PROCEDURES

Cloning, Expression, and Purification of the hVAPB MSP Domains. The DNA fragment encoding the hVAPB MSP domain (residues 1−125) was amplified from a HeLa cell cDNA library by using two designed primers, which was subsequently cloned into a modified pET32a vector (Novagen). The vector was transformed into *Escherichia coli* BL21(DE3) cells (Novagen) for protein expression. The recombinant wild-type MSP protein was first purified by Ni^{2+}-affinity chromatography (Qiagen) under the native condition, followed by in-gel cleavage to remove the His tag. The released MSP protein was further purified on an AKTA FPLC machine (Amersham Biosciences) using a gel filtration column (HiLoad 16/60 Superdex 200), followed by an anion-exchange column (Mono Q 5/50). On the other hand, the Pro56Ser and Pro12Ser mutants were found in the inclusion body, so the pellets were dissolved in the buffer containing 8 M urea and purified with the Ni^{2+}-affinity column under the denaturing condition in the presence of 8 M urea. The eluted fraction was further purified by reverse-phase HPLC on a C4 column and lyophilized. Since the Pro56Ser and Pro12Ser samples precipitated even at pH 4.5 upon addition of thrombin, the His tags were thus not removed as we previously conducted on all other insoluble proteins (*29*−*33*).

The generation of the isotope-labeled proteins for NMR studies followed a similar procedure except that the bacteria were grown in M9 medium with the addition of $(^{15}NH_4)_2SO_4$ for ^{15}N labeling or $(^{15}NH_4)_2SO_4$ and [^{13}C]glucose for ^{15}N and ^{13}C double labeling (*32*, *33*). The purity of all protein samples was checked by the SDS−PAGE gel, and their molecular weights were verified by a Voyager STR matrix-assisted laser desorption ionization time-of-flight mass spectrometer (Applied Biosystems). The concentration of protein samples was determined by the spectroscopic method in the presence of denaturant (*34*).

Crystallization, Data Collection, and Structure Determination. The wild-type MSP domain was prepared at a concentration of 10 mg/mL and crystallized by setting up 2 μL hanging drops at room temperature in a well containing the reservoir solution [25% PEG 3350, 100 mM ammonium acetate, and 0.1 M Tris (pH 7.0)]. The X-ray diffraction images were collected using an in-house Bruker X-ray generator with a wavelength 1.5418 Å equipped with a CCD detector. The structure was determined via the molecular replacement method as previously described (*35*, *36*) using the rVAPA MSP domain structure [Protein Data Bank (PDB) entry 1Z9L] as a search model. The final structure was analyzed by PROCHECK (*37*), and the details are presented in Table 1. Structural coordinates of the wild-type hVAPB MSP domain have been deposited as entry 3IKK. All figures were prepared using the PyMOL molecular graphics system (W. L. DeLano, DeLano Scientific LLC, San Carlos, CA).

Structure and Thermodynamic Stability As Measured by Circular Dichroism. All CD experiments were conducted in a Jasco J-810 spectropolarimeter (Jasco Corp., Tokyo, Japan) as previously described (*30*−*33*). The protein concentration was ~20 μM for all far-UV CD experiments. A very diluted NaOH solution was used to adjust pH valuesm while NaCl was utilized to increase the salt concentration in the Pro56Ser sample in salt-free water. To measure the thermodynamic stability of the

Table 1: Summary of the Crystallographic Analysis of hVAPB MSP[a]

Data Collection	
space group	*R*3
cell dimensions	
a, *b*, *c* (Å)	144.02, 144.02, 34.79
α, *β*, *γ* (deg)	90.0, 90.0, 120.0
resolution (Å)	72.0−2.5 (2.59−2.5)[b]
R_{sym} or R_{merge}	0.104 (0.776)[b]
$I/\sigma I$	8.6 (1.3)[b]
completeness (%)	100 (100)[b]
redundancy	17.41 (14.99)[b]
Refinement	
resolution (Å)	41.5−2.5
no. of reflections	9055
R_{work}/R_{free}	0.2068/0.2655
total no. of atoms	2057
protein	1984
water	73
B factor	34.61
protein	34.13
water	30.34
root-mean-square deviation	
bond lengths (Å)	0.008
bond angles (deg)	1.269

[a]One crystal is used for data collection. [b]Values in parentheses are for the highest-resolution shell.

hVAPB MSP domain, series of far-UV CD spectra were recorded via variation of the urea concentration from 0 to 8 M. Subsequently, we monitored the change in the ellipiticity at 222 nm rather than at 200 nm because the noise at 200 nm became too high to be acceptable at high urea concentrations. Moreover, to increase the signal-to-noise ratio, here we used more concentrated protein samples. The unfolding curve was constructed by plotting the ellipiticity values at 222 nm versus the molar concentration of urea. By assuming a two-state unfolding process, the stability free energy (ΔG°_{N-U}) was determined as previously described (*38*).

ITC Characterization of Binding Activity. Isothermal titration calorimetry (ITC) experiments were performed using a Microcal VP machine as previously described (*36*). The Nir2 peptide (EEEFFDAHE) was purchased from Genesis Biotech Inc. and further purified by HPLC on a reverse-phase C_{18} column. The peptide concentration was determined by the previously described method (*39*) using the fluoraldehyde reagent kit (Thermo Fisher Scientific). Titrations were conducted in the buffer [50 mM Tris-HCl, 150 mM NaCl, and 2 mM DTT (pH 7.5)] at 25 °C. The peptide (300 μM) was loaded into the syringe, while the wild-type hVAPB MSP protein (10 μM) was placed in the sample cell. To obtain thermodynamic binding parameters, the titration data after subtraction of the blank values were fitted to a single-binding site model using the built-in software ORIGIN version 5.0 (Microcal Software Inc.).

NMR Experiments. The wild-type hVAPB MSP sample was prepared in 10 mM phosphate buffer (pH 6.8), while the Pro56Ser and Pro12Ser mutants were dissolved in salt-free water. All NMR data were collected at 25 °C on an 800 MHz Bruker Avance spectrometer equipped with a shielded cryoprobe as described previously (*32*, *36*). For HSQC characterization, samples were prepared at a protein concentration of ∼50 μM. For achieving sequential assignments, triple-resonance experiments, including HNCACB, CBCA(CO)NH, and HNCO, were conducted for both wild-type and Pro56Ser MSP domains on doubly labeled samples at a protein concentration of ∼800 μM. For NOE analysis, ^{15}N-edited HSQC-TOCSY and HSQC-NOESY spectra were recorded for the ^{15}N-labeled Pro56Ser mutant. The ^{1}H chemical shift was referenced directly to 2,2-dimethyl-2-silapentanesulfonic acid (DSS), whereas the ^{15}N and ^{13}C chemical shifts were indirectly referenced to DSS (*40*). The secondary structure mapping based on ^{15}N, HN, CA, CB, CO, and HA chemical shifts was performed using DANGLE in CCPNMR (*41*, *42*).

RESULTS

Structural Properties of the Wild-Type MSP Domain. In this study, we have successfully cloned and expressed the recombinant protein of the wild-type human VAPB (hVAPB) MSP domain (1−125) in *E. coli* cells, which was found in the supernatant. The purified hVAPB MSP domains with and without the His tag were both highly soluble in buffer systems. As shown in Figure 1b, at pH 6.5, the wild-type MSP domain has a far-UV CD spectrum typical of *β*-dominant secondary structure, with the maximal negative signal at ∼218 nm and the positive signal at ∼199 nm (*32*). However, when the pH value is lowered, the intensity of the positive signal at ∼199 nm is reduced gradually. In particular, at pH 3.5, the positive signal at ∼199 nm totally disappeared and the maximal negative signal shifts from ∼218 to ∼212 nm, implying that at pH 3.5, the wild-type MSP domain may be unfolded to some degree.

To gain detailed knowledge about the acid-induced unfolding, we collected series of two-dimensional ^{1}H−^{15}N HSQC spectra on the ^{15}N-labeled wild-type MSP domain with pH values varying from 6.5 to 2.5. Consistent with the CD results, at neutral pH the wild-type MSP domain has a HSQC spectrum typical of a well-folded protein (Figure 1c), with 3.2 and 26 ppm spectral dispersions over the ^{1}H and ^{15}N dimensions, respectively. We have also acquired a HSQC spectrum for the MSP domain with the His tag, and almost all peaks resulting from the MSP residues can be superimposed on those of the MSP domain without the His tag (Figure 1 of the Supporting Information), thus indicating that the presence of the His tag has no detectable effect on the conformation of the MSP domain. On the other hand, as seen in panels c and d of Figure 1, only several HSQC peaks exhibited slight shifts when the solution pH was lowered to 5.5 and 4.5, indicating that no large conformational change occurs for the wild-type MSP domain above pH 4.5, consistent with the CD results. However, when the pH is lowered to 3.5, two sets of peaks manifested in the HSQC spectrum (Figure 1e), implying the coexistence of two conformations. One set of HSQC peaks is very similar to the set at pH 6.5, with very large spectral dispersions, while another newly appeared have a dramatically reduced dispersion which seems to result from an unfolded population. On the basis of the ratio of peak intensities, at pH 3.5 the folded population is estimated to be ∼60% while the unfolded one accounts for ∼40%. When the pH value was further lowered, the intensity of the peaks from the unfolded population increased, and at pH 2.5, only the peak set from the unfolded species could be observed (spectra not shown). However, when the sample pH value was adjusted to 6.5, the unfolded state could fold back to the well-folded state, indicating that the acid-induced unfolding is reversible for the wild-type MSP domain.

Stability and Binding Activity of the Wild-Type MSP Domain. The thermodynamic stability energy is an important factor mediating protein aggregation. Since three free cysteine residues are present in the MSP domain, intermolecular disulfides were found to form at neutral pH and high temperature even in

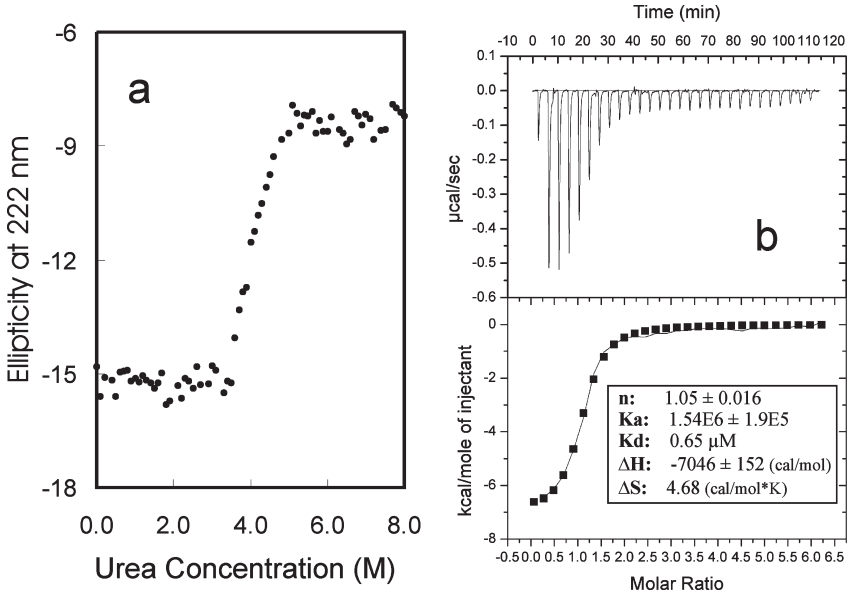

FIGURE 2: Thermodynamic stability and activity of the wild-type MSP domain. (a) Urea-induced unfolding curve as reflected by the change in ellipticity at 222 nm with urea concentrations ranging from 0 to 8 M. (b) ITC profiles of the binding reaction of the wild-type MSP domain with the FFAT motif-containing peptide derived from Nir2 (top) and integrated values for reaction heats with subtraction of the corresponding blank results normalized by the amount of ligand injected vs the molar ratio of MSP/FFAF (bottom). The thermodynamic binding parameters obtained from fitting the data are shown in the box.

the presence of DTT. So here we measured the thermodynamic stability energy using the urea unfolding method (*38*). Briefly, the wild-type MSP domain was unfolded with increasing urea concentrations from 0 to 8 M, and the unfolding process was monitored by measuring the ellipticity change at 222 nm. As seen in Figure 2a, the unfolding process appears to be highly cooperative, starting at the urea concentration of ~3.5 M and ending at ~5.1 M. Fitting of the unfolding data yields a free energy of conformational stability ($\Delta G°_{N-U}$) of 7.40 ± 0.41 kcal/mol. In general, the thermodynamic stability energy for most proteins ranges from 5 to 20 kcal/mol under physiologic conditions (*29*, *43*). This implies that the thermodynamic stability of the wild-type MSP domain is not very high.

Recently, the VAPB MSP domain was demonstrated to functionally interact with the FFAT-containing motif of the Nir2 protein (*10*). Therefore, here we measured thermodynamic parameters for this binding interaction by ITC (Figure 2b). The wild-type MSP domain is able to tightly bind to the FFAT motif-containing peptide EEEFFDAHE derived from the human Nir2 protein, with a dissociation constant (K_D) of 0.65 μM. As such, the CD and ITC results together clearly demonstrate that at neutral pH, the wild-type MSP domain is both structurally well-folded and functionally active.

Crystal Structure of the Wild-Type MSP Domain. To gain further insight into the three-dimensional structure of the wild-type hVAPB MSP domain, we determined its crystal structure at 2.5 Å resolution with a final *R* factor of 0.2068 (R_{free} = 0.2655). Details of the data collection and refinement statistics are summarized in Table 1. In the final model, one asymmetric unit contains two MSP molecules which form a dimer linked through an intermolecular disulfide bridge between two Cys53 residues (Figure 3a). On the other hand, on the basis of the FPLC and DLS characterization, the wild-type hVAPB MSP domain was shown to be a monomer in solution. Interestingly, the same phenomenon has been previously observed in the rat VAPA (rVAPA) MSP domain (*11*). While in solution the rVAPA MSP domain was characterized as a monomer, in crystal it formed a disulfide-bridged dimer with a packing relationship between two monomers very similar to that observed here in the hVAPB MSP structure. Furthermore, the recently deposited NMR structure (entry 2CRI) also shows that the mouse VAPA MSP domain is a monomer in solution. Therefore, as previously concluded for the rVAPA MSP domain (*11*), the dimer observed here in the hVAPB MSP domain structure is also an artifact probably resulting from the crystallization at a very high protein concentration (10 mg/mL).

The two individual molecules in the dimeric hVAPB MSP structure are very similar, with a root-mean-square deviation (rmsd) of only 0.41 Å for the backbone atoms. The hVAPB MSP domain adopts the same fold as the rVAPA MSP domain (PDB entry 1Z9L) with an rmsd of 0.98 Å over the equivalent backbone atoms, composed of seven-strand immunoglobulin-like β sandwiches with s-type topology. Furthermore, only an rmsd of 1.0 Å is obtained over the equivalent backbone atoms if the crystal structures of the hVAPB MSP domain is superimposed with rVAPA MSP domain (PDB entry 1Z9O) in a complex FFAT motif-containing peptide derived from rat ORP1 residues 472−481 (Figure 3b). Also, as seen in Figure 3d, all the rVAPA MSP residues involved in the binding of the ORP1 peptide are conserved in the hVAPB MSP domain. As such, the mode of binding of the hVAPB MSP domain to the FFAT motif-containing peptides is likely similar to that of the rVAPA MSP to the ORP1 peptide.

One of the most characteristic structural properties of the hVAPB MSP domain is the existence of two S-shaped loops over the Gln11-Pro12-Gln13-His14 and Arg55-Pro56-Asn57-Ser58 regions, which appear to be stabilized by the cis-peptide bond conformation constrained by Pro12 and Pro56, respectively (Figure 3c). The first S-shaped loop connects the Ser9-Leu10 and Glu15−Arg19 β-strands, whereas the second S-shaped loop connects the Cys53-Val54 and Gly59−Ile61 β-strands (Figure 3d). By examining the crystal structure and analyzing the NOE pattern between Pro12 and Pro56 and preceding residues, we also found those two unique S-shaped loops in both crystal and

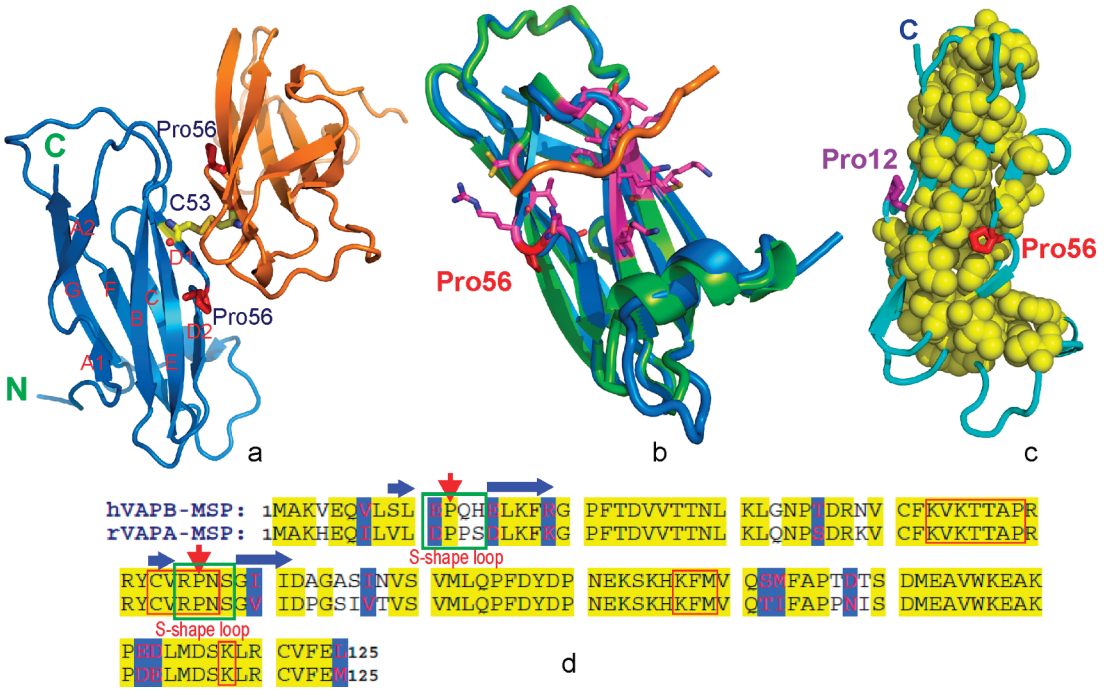

FIGURE 3: Crystal structure of the wild-type MSP domain. (a) Dimeric crystal structure of the wild-type hVAPB MSP domain (PDB entry 3IKK) linked by an intermolecular disulfide bridge between two Cys53 residues. It shares the same fold as the rVAPA MSP domain (PDB entry 1Z9L), composed of seven-strand immunoglobulin-like β sandwiches with s-type topology. The β strands are labeled in one molecule, and Pro56 side chains are displayed as sticks. (b) Structural superimposition of the hVAPB MSP and rVAPA MSP (PDB entry 1Z9O) domains in complex with an ORP1 peptide containing the FFAT motif. The rVAPA residues involved in direct contacts with the peptide are displayed as sticks. Pro56 located at one end of the binding pocket is also shown as red sticks. (c) hVAPB MSP structure shown as a blue ribbon, with hydrophobic residues displayed as yellow spheres and Pro56 as red sticks. (d) Sequence alignment of the hVAPB and rVAPA MSP domains, with residues on the binding interface with the peptide boxed.

NMR structures of the rat VAPA MSP domains. In particular, it has been suggested that because it is critically located in the S-shaped loop, Pro56 might play a key role in stabilizing the MSP domain and consequently its mutation would result in insolubility (*22*). Intriguingly, we have examined all available structures of major sperm proteins and found that those two S-shaped loops were also conserved in them.

Structural Consequences of the Pro56Ser Mutation. To address the consequence of the ALS-causing Pro56Ser mutation, we generated the Pro56Ser mutant of the hVAPB MSP domain by using site-directed mutagenesis. Surprisingly, the recombinant Pro56Ser protein was found to exist only in inclusion bodies, and our attempts by fast dilution and dialysis to refold it in buffer systems all failed because of severe precipitation. Previously, these insoluble proteins could not be assessed by high-resolution biophysical methods. However, we recently discovered these "insoluble proteins" could in fact be solubilized in salt-free water (*29*−*33*), and now this approach has also been used by other groups to characterize insoluble proteins (*44*−*47*). Therefore, we purified the Pro56Ser mutant from inclusion bodies with a Ni^{2+}-affinity column under the denaturing condition in the presence of 8 M urea, followed by further HPLC purification on a reverse-phase C4 column. Again the lyophilized Pro56Ser protein could be dissolved in salt-free water at high concentrations. The protein sample directly dissolved in milli-Q water has a pH value of ~3.5 because of the remaining TFA (trifluoroacetic acid) from the HPLC solvent.

As shown in Figure 4a, at pH 3.5 the Pro56Ser MSP domain has a far-UV CD spectrum characteristic of a predominantly unstructured protein, with its maximal negative signal at ~199 nm and without any positive signal (*30*). Interestingly, the overall shapes of the CD curves are very similar at pH 3.5, 4.5, and 5.5, indicating that the mutant remains highly unstructured even at pH 5.5. However, even at a protein concentration of ~20 μM, when we attempted to increase the solution pH further to 6.5, the CD sample became cloudy immediately and its CD signal became very weak. We have also explored the effect of salt on the conformational properties of the Pro56Ser mutant by far-UV CD. As shown in Figure 4b, the overall shapes of the CD spectra are still similar at various pH values and salt concentrations up to 10 mM, indicating that the mutant remains similarly disordered under these conditions. However, when the pH value reached 6.5 for the sample containing 10 mM salt, the protein precipitated immediately, and consequently, the CD signal disappeared (Figure 4b). We have also addressed the dynamic aggregation by collecting the far-UV CD and NMR HSQC spectra at different protein concentrations. At pH < 4.0, no significant concentration dependence was observed for the shape and intensity of CD curves or the chemical shift and line width of HSQC spectra. Furthermore, NMR resonance peaks could be observed without significant broadening in other heteronuclear NMR spectra, including triple-resonance experiments, HSQC-TOCSY and HSQC-NOESY. These results together imply that no significant aggregation occurred at low pH values.

We also assessed the effects of pH and salt on the conformational properties of the Pro56Ser mutant using NMR HSQC spectroscopy. As one can see in Figure 4c, at pH 3.5, the mutant has a HSQC spectrum characteristic of an unfolded protein without any tight tertiary packing, with only 0.8 and 11 ppm dispersions over the ^{1}H and ^{15}N dimensions, respectively (*43*−*46*), consistent with the CD results. Interestingly, at pH 3.5 many HSQC peaks of the mutant can be superimposed with those from

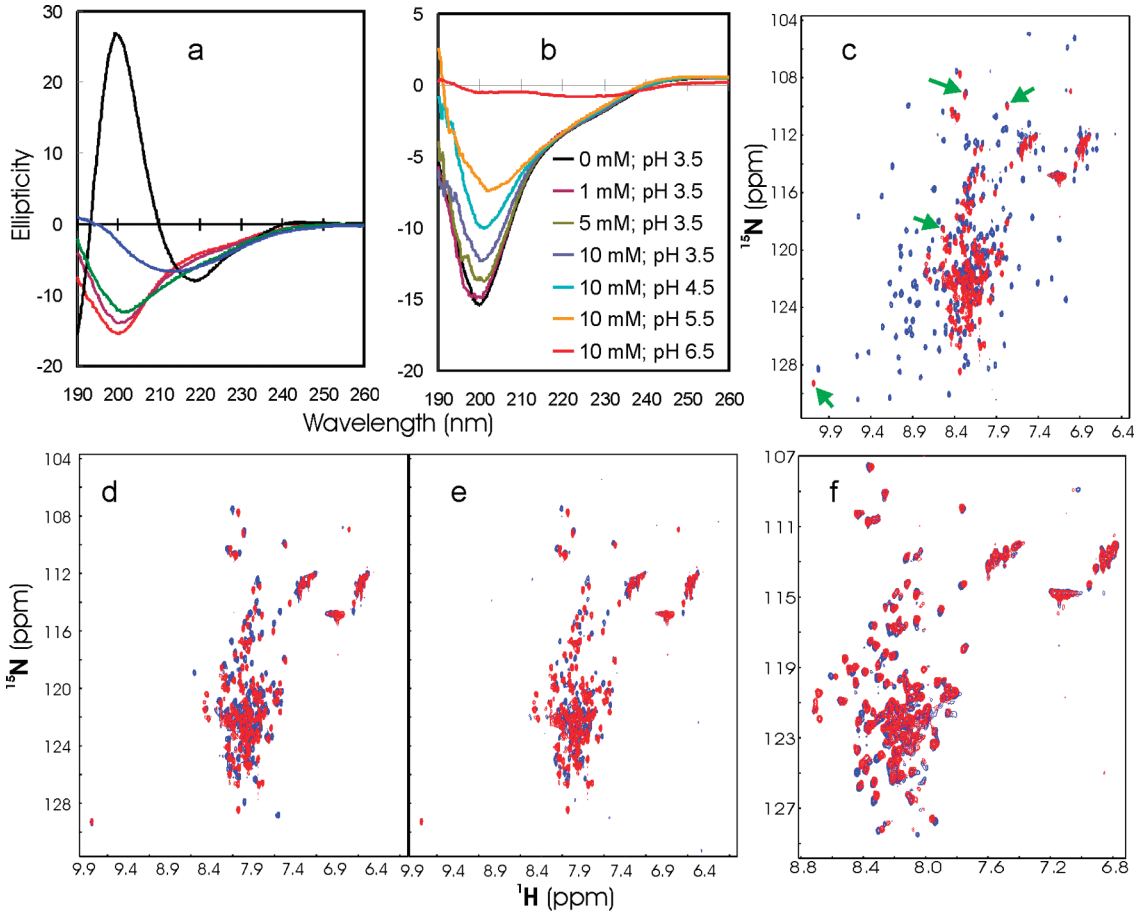

FIGURE 4: Structural consequences of the Pro56Ser mutation. (a) Far-UV CD spectra of the wild-type MSP (black) and Pro56Ser mutant at pH 3.5 (red), 4.5 (brown), 5.5 (green), and 6.5 (blue). (b) Far-UV CD spectra of the Pro56Ser mutant at different pH values and salt concentrations. (c) Superimposition of the HSQC spectra of the wild-type MSP domain (blue) and Pro56Ser mutant at pH 3.5 (red). Green arrows are used to indicate some superimposed HSQC peaks. (d) Superimposition of the HSQC spectra of the Pro56Ser mutant at pH 4.5 (blue) and 3.5 (red). (e) Superimposition of the HSQC spectra of the Pro56Ser mutant at pH 5.5 (blue) and 3.5 (red). (f) Superimposition of the HSQC spectra of the Pro56Ser mutant at pH 3.5 in the absence (red) and presence (blue) of 20 mM salt.

the unfolded population of the wild type at pH 3.5 (Figure 4c). It is thus interesting to investigate whether the mutant might have a conformational ensemble similar to that of the unfolded population of the wild type at pH 3.5. However, unlike the wild-type MSP domain which could reversibly fold back at pH >4.5, the Pro56Ser mutant at pH 4.5 and 5.5 still remains highly unstructured as no significant dispersion change is observed for their HSQC spectra (Figure 4d,e). At pH 6.5, the protein completely aggregated, and consequently, no HSQC peaks could be detected (data not shown). On the other hand, at pH 3.5 an HSQC spectrum could be collected on the Pro56Ser sample in the presence of 20 mM NaCl (Figure 4f). No significant change in spectral dispersions occurs, and only some peaks undergo slight shifts probably due to the nonspecific interactions with the salt ions, suggesting that the salt has no considerable effect on the conformation of the Pro56Ser mutant.

Residue-Specific Conformational Properties of the Pro56Ser Mutant. The successful solubilization of the Pro56Ser protein offered an unprecedented opportunity to examine its residue-specific conformational properties. To achieve this, we have isotopically labeled both the wild-type and Pro56Ser MSP domains and acquired a large set of three-dimensional heteronuclear NMR spectra. Because at the very high protein concentrations required for these NMR experiments, varying the pH value and salt concentration would lead to severe line broadening or even precipitation, all three-dimensional NMR experiments with the Pro56Ser mutant were performed at pH 3.5 in salt-free water.

For the wild-type MSP domain, NMR HSQC resonance peaks were detected and assigned for almost all residues except for several short stretches (Gln11−His14, Ser84−Lys87, and Lys110−Glu112). For the Pro56Ser mutant, probably due to more severe conformational exchanges on the microsecond to millisecond time scale or/and dynamic aggregation in the unfolded state, more NMR HSQC resonance peaks were invisible, including the Ala48−Arg51, Met72−Gln74, Pro80−Phe94, Pro111−Ser117, and Val122−Leu125 fragments. Since the chemical shift values might be slightly imprecise for a variety of reasons (*48*), we also tested the recalibration of the CA and CB chemical shifts using the proposed procedure (*48*), but only a minor difference of 0.09 ppm was obtained.

Figure 5 presents CA, CO, and HA chemical shift deviations from their random-coil values for both native and Pro56Ser MSP domains. It has been well-established that these deviations are very sensitive indicators of protein secondary structures, thus representing a powerful probe for the detection of residual secondary structures in unfolded or partially folded proteins (*49*−*51*). As seen in Figure 5, the wild-type MSP domain has very large CA and CO deviations typical of a fully folded protein, while the Pro56Ser mutant has dramatically reduced deviations characteristic of an unfolded protein. Very surprisingly, it appears that in the Pro56Ser mutant, the native β-sheet secondary structure

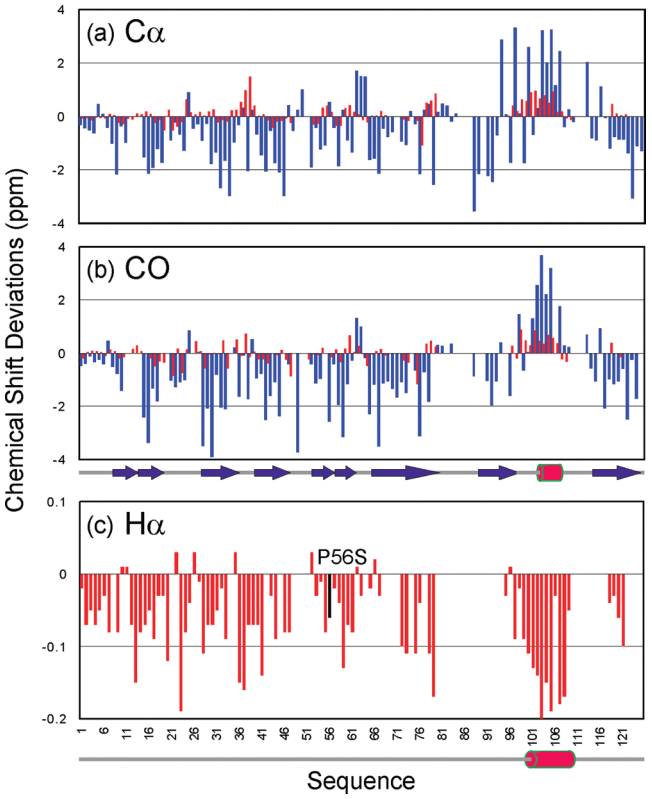

FIGURE 5: Residue-specific conformational properties. Bar plot of chemical shift deviations ($\Delta\delta = \delta_{obs} - \delta_{coil}$) of Cα (a), CO (b), and Hα (c) atoms from their random-coil values for the wild-type (blue) and Pro56Ser (red) domains. The black bar is used to indicate the Pro56Ser mutation. The secondary structures of the Pro56Ser mutant are mapped by DANGLE to be predominantly random coil for almost all the sequence except for the presence of a weakly populated helix (red cylinder) over residues Thr97−Glu108.

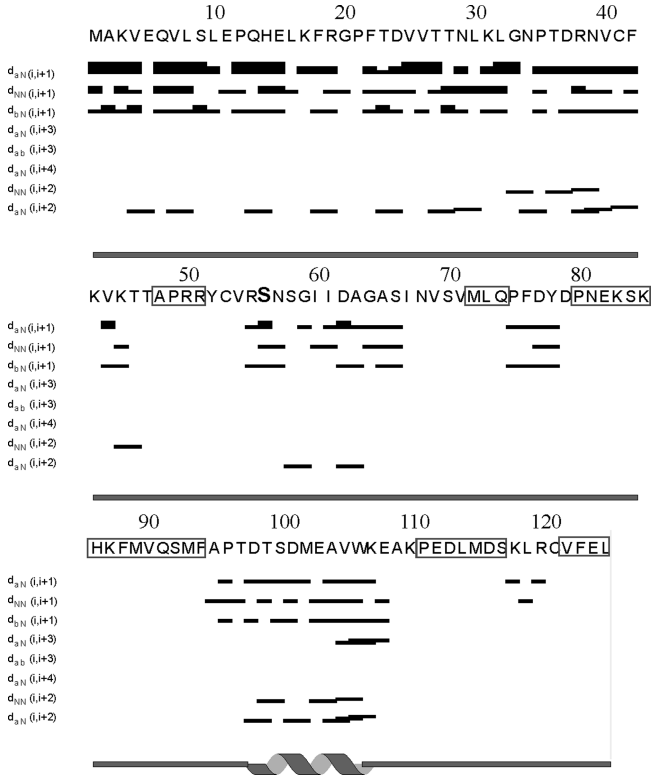

FIGURE 6: Characteristic NOEs defining secondary structure. NOE connectivities identified for the Pro56Ser mutant. Plots were generated by CCPNMR. The boxed residues cannot be detected in the HSQC spectrum and thus are not assigned.

is totally eliminated. Instead, on the basis of the negative HA chemical shift deviations (Figure 5c), it appears that the non-native helical conformation is weakly populated over the sequence. However, small deviations (all ≤0.2 ppm) also indicate that in the Pro56Ser mutant, the helical population is very low as compared to what we previously observed on a partially folded SH3 domain (*32*).

Moreover, we used DANGLE, which was shown to be more tolerant to the imperfect calibration of chemical shifts (*42*), to map the secondary structures based on chemical shift deviations. The results indicate that in solution the wild-type hVAPB MSP domain has secondary structure patterns completely consistent with those in the crystal structure. By contrast, the Pro56Ser mutant has random-coil conformation almost over the whole sequence except for the presence of a weakly populated helix over residues Thr97−Glu108 (Figure 5c). Interestingly, in the wild-type MSP structure, a helix is also formed, but it is much shorter, only spanning residues Ala104−Glu108.

We have also analyzed the ^{15}N-edited HSQC-NOESY spectrum, but no long-range NOEs could be identified, strongly suggesting the absence of any stable tertiary packing in the Pro56Ser mutant. As shown in Figure 6, except for the missing residues, sequential $d_{NN}(i, i + 1)$ and medium-range $d_{\alpha N}(i, i + 2)$ NOEs could be observed over the majority of the sequence, suggesting that the nonhelical conformation is indeed populated to some degree. However, $d_{NN}(i, i + 2)$ NOEs could be found only over two segments (Gly33−Thr46 and Thr97−Glu108), while only two $d_{\alpha N}(i, i + 3)$ NOEs could be identified between Ala104 and Lys107 and between Val105 and Glu108. These results, together with a complete lack of any $d_{\alpha N}(i, i + 4)$ NOE, imply that the non-native helical conformation is very dynamic and only weakly populated in the Pro56Ser mutant (*32*, *33*).

Finally, we have also used NMR HSQC titrations to examine whether the Pro56Ser mutant is still able to bind to the Nir2 peptide in solution. However, the obtained result demonstrates that there is no detectable binding at pH 3.5 even in the presence of 10 mM salt, even at a molar ratio of up to 1:50 [Pro56Ser:peptide (results not shown)]. Unfortunately, further attempts to detect the binding interaction at higher pH values failed because of severe aggregation upon peptide addition.

Structural Consequences of the Pro12Ser Mutation. Two characteristic S-shaped loops are present in the hVAPB MSP domain, and here we have experimentally demonstrated that Pro56 indeed plays an essential role in maintaining the MSP structure. To explore whether Pro12 also plays a similar role, we mutated Pro12 to Ser by using site-directed mutagenesis. Very strikingly, the Pro12Ser mutant indeed became insoluble and was only found in the inclusion body. As such, we obtained the recombinant Pro12Ser protein via Ni^{2+}-affinity purification under denaturing conditions followed by RP-HPLC purification. As judged by the CD results in salt-free water (Figure 7a), Pro12Ser is highly unstructured at pH < 5.5 but becomes severely aggregated at pH 6.5. This is further supported by the HSQC spectra at different pH values. At pH 6.5, no HSQC peaks could be detected even with the spectral contour down to the noise level (Figure 7e), suggesting a drastic aggregation at this pH. On the other hand, many HSQC peaks of the Pro12Ser mutant can be superimposed with those of the Pro56Ser mutant (Figure 6b), implying that the Pro12Ser and Pro56Ser mutants might have similar conformational properties over a large portion of the molecules.

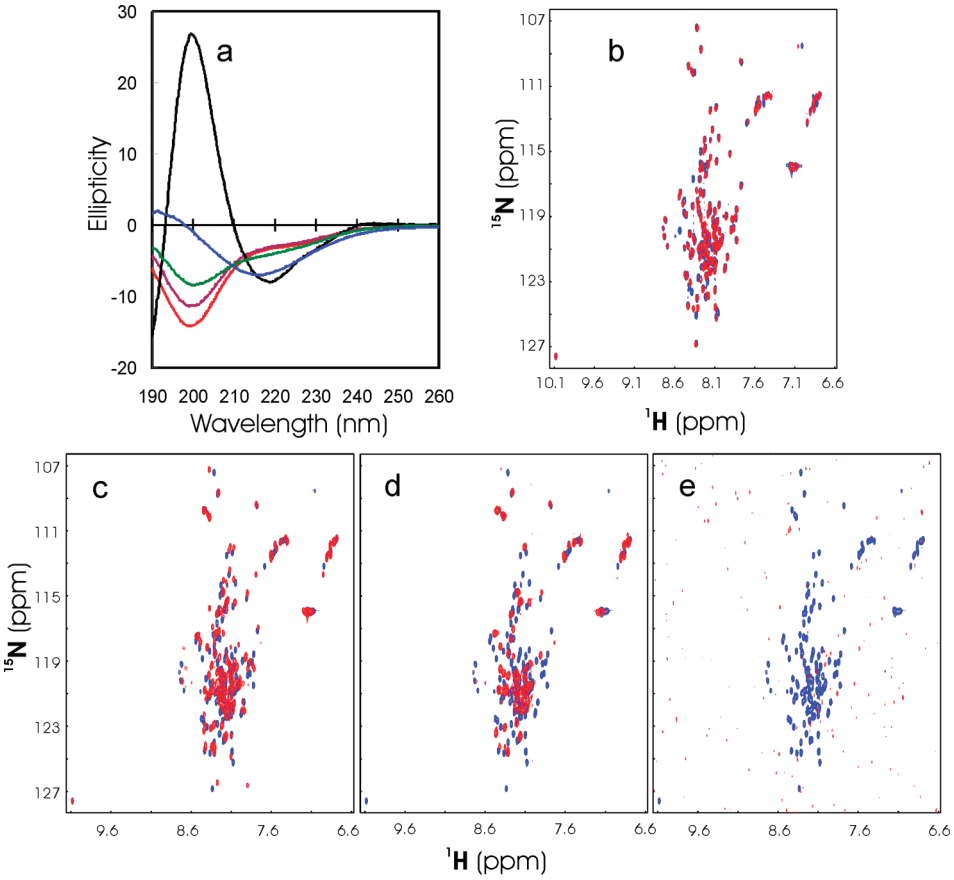

FIGURE 7: Structural consequences of the Pro12Ser mutation. (a) Far-UV CD spectra of the wild-type MSP (black) and Pro12Ser mutant in salt-free water at pH 3.5 (red), 4.5 (brown), 5.5 (green), and 6.5 (blue). (b) Superimposition of the HSQC spectra of the Pro56Ser (blue) and Pro12Ser mutants in salt-free water at pH 3.5 (red). (c) Superimposition of the HSQC spectra of the Pro12Ser mutant in salt-free water at pH 3.5 (blue) and 4.5 (red). (d) Superimposition of the HSQC spectra of the Pro56Ser mutant in salt-free water at pH 3.5 (blue) and 5.5 (red). (e) Superimposition of the HSQC spectra of the Pro56Ser mutant in salt-free water at pH 3.5 (blue) and 6.5 (red).

DISCUSSION

Amyotrophic lateral sclerosis (ALS) was described more than 130 years ago, but its underlying mechanism still remains a mystery. In fact, our current knowledge of the pathobiology of ALS is largely derived from studies of ALS1-associated gene mutations. So far, more than 125 mutations of SOD1 have been identified, and exhaustive biophysical studies on them have provided mechanistic insights into the molecular events associated with the development of ALS (*52*, *53*).

Recently, from a large Brazilian family, a Pro56Ser point mutation on the hVAPB MSP domain has been identified to cause a familial amyotrophic lateral sclerosis. However, so far, no study on the structure and stability of the wild-type MSP domain has been reported, and in particular, the structural consequences of this mutation remain completely unknown. Here, our obtained results demonstrate that the wild-type hVAPB MSP domain is well-folded at neutral pH, with a three-dimensional structure highly similar to that of the rVAPA MSP domain. Interestingly, the wild-type MSP domain can undergo a reversible acid-induced unfolding which appears to be highly cooperative between two states, unlike the gradual unfolding we previously observed (*54*, *55*). Furthermore, the wild-type MSP domain is fully active in tightly binding to the FFAT motif containing a peptide derived from the Nir2 protein, with a K_D of 0.65 μM. This binding action has been functionally demonstrated to regulate ER structure (*10*). On the other hand, the wild-type MSP domain has a stability free energy of 7.40 kcal/mol, which is not very large as the thermodynamic stability for most proteins ranges from 5 to 20 kcal/mol under physiological conditions (*29*, *34*).

Most importantly, the successful solubilization of the insoluble Pro56Ser mutant allows visualization of its residue-specific conformational properties. Very surprisingly, this point mutation not only disrupts the tight tertiary packing but also eliminates all native β-sheet secondary structures in the wild-type MSP domain. On the basis of chemical shift deviations and the NOE pattern, it appears that in the mutant, only helical conformation is weakly populated over the sequence and a dynamic helical segment was identified by DANGLE to exist over residues Thr97−Glu108. Previously, the formation of the non-native helical conformation in a β-dominant protein was thought to be advantageous because it serves as a landmark to restrict the folding route, favoring further transformation into the native β-sheet structure (*56*−*59*). Via detailed NMR investigations, we recently revealed that the non-native helical conformation is indeed highly populated in a partially folded SH3 domain (*32*, *33*).

Our results clearly demonstrate that the Pro56Ser mutant continues to lack a native structure under a variety of pH values and salt concentrations. This implies that the Pro56Ser mutation is able to eliminate the ability of the mutated sequence to fold into the native structure adopted by the wild-type MSP sequence. So why is a single amino acid mutation, Pro56Ser, able to trigger such a remarkable consequence? As seen in Figure 3c, as in most well-folded proteins, in the wild-type MSP domain, the side chains of the hydrophobic residues are buried and form a compact core seemingly critical for stabilizing the folded conformation

as we previously observed for CHABII protein (*54*, *55*). Interestingly, the residue Pro56 is sitting at the central position of the hydrophobic core. Furthermore, previously Pro56 was thought to play a key role in stabilizing the MSP structure because it was located in the characteristic S-shaped loop, adopting the unusual cis-peptide bond conformation in the rVAPA MSP domain (*22*). As such, the replacement of the hydrophobic Pro56 with the polar Ser is anticipated to impose two effects: (1) to abolish the S-shaped loop and significantly increase the backbone flexibility around Pro56 and (2) to destabilize the hydrophobic core upon introduction of the polar side chain of Ser (*22*, *54*, *55*, *60*). The importance of the two S-shaped loops in maintaining the structural integrity of the MSP domain is further supported by our experimental results about the abolishment of its structure and solubility as triggered by the Pro12Ser mutation. Because the thermodynamic stability of the hVAPB MSP domain is not very large, the two destabilizing effects appear to be sufficient to abolish the ability of the mutant sequence to form the native structure of the wild-type MSP domain.

On the other hand, as we previously showed with other insoluble proteins (*29*−*33*, *61*), in the Pro56Ser and Pro12Ser MSP domains, the abolishment of the tight tertiary structure will result in the exposure of hydrophobic side chains. These exposed hydrophobic side chains have a strong tendency to be clustered together to form aggregates, unless the attractive hydrophobic interaction can be suppressed by the intrinsic repulsive electrostatic interactions in salt-free water, with the solution pH several units from the protein isoelectric point (pI) (*29*). Indeed, the pI values of the Pro56Ser and Pro12Ser mutants were estimated to be ~7.5, thus explaining the observation that the Pro56Ser and Pro12Ser proteins would precipitate immediately after the solution pH was adjusted to neutral. On the other hand, under physiological conditions, the pH is ~7.0 and the concentration of the salt ions is ~150 mM. As a result, at physiologically relevant pH values, the repulsive electrostatic interactions are relatively weak and also will be further screened out by the presence of ~150 mM salt. Consequently, in vivo, the hydrophobic interaction will become dominant in the Pro56Ser mutant because of both the neutral pH and the high salt concentration, thus resulting in severe aggregation (*29*−*33*, *61*). This thus rationalizes the previous observation that in vivo, the Pro56Ser mutant formed very tight aggregates that were even resistant to solubilization by buffers containing nonionic detergents such as Triton X-100 (*22*).

Here we propose that the mechanism for aggregation of the Pro56Ser mutant may represent a general one underlying aggregation of other disease-related proteins triggered by genetic mutation or posttranslational modification. Basically, the mutation or modification at strategic positions may dramatically eliminate the ability of the mutant sequences to fold into the stable and well-folded structures adopted by the wild-type sequences (*33*, *60*). As a consequence, the partially folded or highly disordered mutants with many hydrophobic side chains exposed can only be dissolved in salt-free water but not in buffers mimicking the physiological condition. Finally, our present success again highlights the promising potential to use salt-free water to solubilize buffer insoluble proteins for high-resolution biophysical investigations to improve our understanding of mechanisms of protein folding and aggregation characteristic of a large array of human diseases (*62*, *63*).

In conclusion, our study shows for the first time that the Pro56Ser hVAPB MSP domain is lacking a well-folded native structure. Consequently, it may have many hydrophobic side chains exposed and would form highly insoluble aggregates under physiological conditions as recently observed in vivo. Also, because of the complete abolishment of the native MSP structure, the Pro56Ser mutant is most unlikely to retain any functions requiring its native structure, such as the involvement in lipid metabolism, protein transport, maintenance of ER structure, mediation of unfolded protein response (UPR) in the ER, and binding to Eph receptors. The loss of all or part of these functions may account for the development of ALS. Alternatively or/and additionally, a significant accumulation of the Pro56Ser aggregates may also activate ER stress-induced apoptosis which has recently been demonstrated to be critical for some neurodegenerative diseases (*64*, *65*). In the future, it is also interesting to screen whether some ALS patients carry the Pro12Ser mutation and/or to explore whether the Pro12Ser mutation will also lead to ALS in animal models.

SUPPORTING INFORMATION AVAILABLE

One supplementary figure showing superimposition of the HSQC spectra at pH 6.5 on an 800 MHz Bruker spectrometer for the wild-type hVAPB MSP domains with (blue) and without (red) the His tag. This material is available free of charge via the Internet at http://pubs.acs.org.

REFERENCES

1. Bruijn, L. I., Miller, T. M., and Cleveland, D. W. (2004) Unraveling the mechanisms involved in motor neuron degeneration in ALS. *Annu. Rev. Neurosci. 27*, 723–749.
2. Pasinelli, P., and Brown, R. H. (2006) Molecular biology of amyotrophic lateral sclerosis: Insights from genetics. *Nat. Rev. Neurosci. 7*, 710–723.
3. Nishimura, A. L., Mitne-Neto, M., Silva, H. C., Richieri-Costa, A., Middleton, S., Cascio, D., Kok, F., Oliveira, J. R., Gillingwater, T., Webb, J., Skehel, P., and Zatz, M. (2004) A mutation in the vesicle-trafficking protein VAPB causes late onset spinal muscular atrophy and amyotrophic lateral sclerosis. *Am. J. Hum. Genet. 75*, 822–831.
4. Nishimura, A. L., Al-Chalabi, A., and Zatz, M. (2005) A common founder for amyotrophic lateral sclerosis type 8 (ALS8) in the Brazilian population. *Hum. Genet. 118*, 499–500.
5. Hirano, M. (2008) VAPB: New genetic clues to the pathogenesis of ALS. *Neurology 70*, 1161–1162.
6. Skehel, P. A., Martin, K. C., Kandel, E. R., and Bartsch, D. (1995) A VAMP-binding protein from Aplysia required for neurotransmitter release. *Science 269*, 1580–1583.
7. Nishimura, Y., Hayashi, M., Inada, H., and Tanaka, T. (1999) Molecular cloning and characterization of mammalian homologues of vesicle-associated membrane protein-associated (VAMP-associated) proteins. *Biochem. Biophys. Res. Commun. 254*, 21–26.
8. Skehel, P. A., Fabian-Fine, R., and Kandel, E. R. (2000) Mouse VAP33 is associated with the endoplasmic reticulum and microtubules. *Proc. Natl. Acad. Sci. U.S.A. 97*, 1101–1106.
9. Soussan, L., Burakov, D., Daniels, M. P., Toister-Achituv, M., Porat, A., Yarden, Y., and Elazar, Z. (1999) ERG30, a VAP-33-related protein, functions in protein transport mediated by COPI vesicles. *J. Cell Biol. 146*, 301–311.
10. Amarilio, R., Ramachandran, S., Sabanay, H., and Lev, S. (2005) Differential regulation of endoplasmic reticulum structure through VAP-Nir protein interaction. *J. Biol. Chem. 280*, 5934–5944.
11. Kaiser, S. E., Brickner, J. H., Reilein, A. R., Fenn, T. D., Walter, P., and Brunger, A. T. (2005) Structural basis of FFAT motif-mediated ER targeting. *Structure 13*, 1035–1045.
12. Loewen, C. J., and Levine, T. P. (2005) A highly conserved binding site in vesicle-associated membrane protein-associated protein (VAP) for the FFAT motif of lipid-binding proteins. *J. Biol. Chem. 280*, 14097–14104.
13. Olkkonen, V. M. (2004) Oxysterol binding protein and its homologues: New regulatory factors involved in lipid metabolism. *Curr. Opin. Lipidol. 15*, 321–327.
14. Holthuis, J. C., and Levine, T. P. (2005) Lipid traffic: Floppy drives and a superhighway. *Nat. Rev. Mol. Cell Biol. 6*, 209–220.

15. Levine, T., and Loewen, C. (2006) Inter-organelle membrane contact sites: Through a glass, darkly. *Curr. Opin. Cell Biol. 18*, 371–378.
16. Kawano, M., Kumagai, K., Nishijima, M., and Hanada, K. (2006) Efficient trafficking of ceramide from the endoplasmic reticulum to the Golgi apparatus requires a VAMP-associated protein-interacting FFAT motif of CERT. *J. Biol. Chem. 281*, 30279–30288.
17. Perry, R. J., and Ridgway, N. D. (2006) Oxysterol-binding protein and vesicle-associated membrane protein-associated protein are required for sterol dependent activation of the ceramide transport protein. *Mol. Biol. Cell 17*, 2604–2616.
18. Wyles, J. P., McMaster, C. R., and Ridgway, N. D. (2002) Vesicle-associated membrane protein-associated protein-A (VAP-A) interacts with the oxysterol-binding protein to modify export from the endoplasmic reticulum. *J. Biol. Chem. 277*, 29908–29918.
19. Weir, M. L., Xie, H., Klip, A., and Trimble, W. S. (2001) VAP-A binds promiscuously to both v- and tSNAREs. *Biochem. Biophys. Res. Commun. 286*, 616–621.
20. Tsuda, H., Han, S. M., Yang, Y., Tong, C., Lin, Y. Q., Mohan, K., Haueter, C., Zoghbi, A., Harati, Y., Kwan, J., Miller, M. A., and Bellen, H. J. (2008) The amyotrophic lateral sclerosis 8 protein VAPB is cleaved, secreted, and acts as a ligand for Eph receptors. *Cell 133*, 963–977.
21. Mitne-Neto, M., Ramos, C. R., Pimenta, D. C., Luz, J. S., Nishimura, A. L., Gonzales, F. A., Oliveira, C. C., and Zatz, M. (2007) A mutation in human VAP-B−MSP domain, present in ALS patients, affects the interaction with other cellular proteins. *Protein Expression Purif. 55*, 139–146.
22. Teuling, E., Ahmed, S., Haasdijk, E., Demmers, J., Steinmetz, M. O., Akhmanova, A., Jaarsma, D., and Hoogenraad, C. C. (2007) Motor neuron disease-associated mutant vesicle-associated membrane protein-associated protein (VAP) B recruits wild-type VAPs into endoplasmic reticulum-derived tubular aggregates. *J. Neurosci. 27*, 9801–9815.
23. Ratnaparkhi, A., Lawless, G. M., Schweizer, F. E., Golshani, P., and Jackson, G. R. (2008) A *Drosophila* model of ALS: Human ALS-associated mutation in VAP33A suggests a dominant negative mechanism. *PLoS One 3*, e2334.
24. Prosser, D. C., Tran, D., Gougeon, P. Y., Verly, C., and Ngsee, J. K. (2008) FFAT rescues VAPA-mediated inhibition of ER-to-Golgi transport and VAPB-mediated ER aggregation. *J. Cell Sci. 121* (Part 18), 3052–3061.
25. Kanekura, K., Nishimoto, I., Aiso, S., and Matsuoka, M. (2006) Characterization of amyotrophic lateral sclerosis-linked P56S mutation of vesicle-associated membrane protein-associated protein B (VAPB/ALS8). *J. Biol. Chem. 281*, 30223–30233.
26. Gkogkas, C., Middleton, S., Kremer, A. M., Wardrope, C., Hannah, M., Gillingwater, T. H., and Skehel, P. (2008) VAPB interacts with and modulates the activity of ATF6. *Hum. Mol. Genet. 17*, 1517–1526.
27. Kanekura, K., Suzuki, H., Aiso, S., and Matsuoka, M. (2009) ER Stress and Unfolded Protein Response in Amyotrophic Lateral Sclerosis. *Mol. Neurobiol. 39*, 81–89.
28. Suzuki, H., Kanekura, K., Levine, T. P., Kohno, K., Olkkonen, V. M., Aiso, S., and Matsuoka, M. (2009) ALS-linked P56S-VAPB, an aggregated loss-of-function mutant of VAPB, predisposes motor neurons to ER stress-related death by inducing aggregation of co-expressed wild-type VAPB. *J. Neurochem. 108*, 973–985.
29. Song, J. (2009) Insight into "Insoluble Proteins" with Pure Water. *FEBS Lett. 583*, 953–959.
30. Li, M., Liu, J., Ran, X., Fang, M., Shi, J., Qin, H., Goh, J. M., and Song, J. (2006) Resurrecting Abandoned Proteins with the Pure Water: CD and NMR studies of protein fragments solubilized in salt-free water. *Biophys. J. 91*, 4201–4209.
31. Li, M., Liu, J., and Song, J. (2006) Nogo goes in the pure water: Solution structure of Nogo-60 and design of the structured and buffer-soluble Nogo-54 for enhancing CNS regeneration. *Protein Sci. 15*, 1835–1841.
32. Liu, J., and Song, J. (2008) NMR Evidence for Forming Highly-Populated Helical Conformations in the Partially-Folded hNck2 SH3 Domain. *Biophys. J. 95*, 4803–4812.
33. Liu, J., and Song, J. (2009) Insights into Protein Aggregation by NMR Characterization of Insoluble SH3 Mutants Solubilized in Salt-Free Water. *PLoS One 4*, e7805.
34. Pace, C. N., Vajdos, F., Fee, L., Grimsley, G., and Gray, T. (1995) How to measure and predict the molar absorption coefficient of a protein. *Protein Sci. 4*, 2411–2423.
35. Shi, J., Sivaraman, J., and Song, J. (2008) Mechanism for Controlling Dimer-monomer Switch and Coupling Dimerization to Catalysis of the SARS-CoV 3C-Like Protease. *J. Virol. 82*, 4620–4629.
36. Qin, H., Shi, J., Noberini, R., Pasquale, E. B., and Song, J. (2008) Crystal Structure and NMR Binding Reveal That Two Small Molecule Antagonists Target the High Affinity Ephrin-binding Channel of the EphA4 Receptor. *J. Biol. Chem. 283*, 29473–29484.
37. Laskowski, R. A., Rullmannn, J. A., MacArthur, M. W., Kaptein, R., and Thornton, J. M. (1996) AQUA and PROCHECK-NMR: Programs for checking the quality of protein structures solved by NMR. *J. Biomol. NMR 8*, 477–486.
38. Gupta, R., Yadav, S., and Ahmad, F. (1996) Protein stability: Urea-induced versus guanidine induced unfolding of metmyoglobin. *Biochemistry 35*, 11925–11930.
39. Panasiuk, R., Amarowicz, R., Kostyra, H., and Sijtsma, L. (1998) Determination of α-amino nitrogen in pea protein hydrolysates: A comparison of three analytical methods. *Food Chem. 62*, 363–367.
40. Wishart, D. S., Bigam, C. G., Yao, J., Abildgaard, F., Dyson, H. J., Oldfield, E., Markley, J. L., and Sykes, B. D. (1995) ^{1}H, ^{13}C and ^{15}N chemical shift referencing in biomolecular NMR. *J. Biomol. NMR 6*, 135–140.
41. Vranken, W. F., Boucher, W., Stevens, T. J., Fogh, R. H., Pajon, A., Llinas, M., Ulrich, E. L., Markley, J. L., Ionides, J., and Laue, E. D. (2005) The CCPN data model for NMR spectroscopy: Development of a software pipeline. *Proteins 59*, 687–696.
42. Cheung, M. S., Maguire, M. L., Stevens, T. J., and Broadhurst, R. W. (2010) DANGLE: A Bayesian inferential method for predicting protein backbone dihedral angles and secondary structure. *J. Magn. Reson. 202*, 223–233.
43. Chi, E. Y., Krishnan, S., Randolph, T. W., and Carpenter, J. F. (2003) Physical stability of proteins in aqueous solution: Mechanism and driving forces in nonnative protein aggregation. *Pharm. Res. 20*, 1325–1336.
44. Delak, K., Harcup, C., Lakshminarayanan, R., Sun, Z., Fan, Y., Moradian-Oldak, J., and Evans, J. S. (2009) The Tooth Enamel Protein, Porcine Amelogenin, Is an Intrinsically Disordered Protein with an Extended Molecular Configuration in the Monomeric Form. *Biochemistry 48*, 2272–2281.
45. Delak, K., Collino, S., and Evans, J. S. (2009) Polyelectrolyte Domains and Intrinsic Disorder within the Prismatic Asprich Protein Family. *Biochemistry 48*, 3669–3677.
46. Amos, F. F., and Evans, J. S. (2009) AP7, a partially disordered pseudo C-RING protein, is capable of forming stabilized aragonite in vitro. *Biochemistry 48*, 1332–1339.
47. Aguado-Llera, D., Goormaghtigh, E., de Geest, N., Quan, X. J., Prieto, A., Hassan, B. A., Gómez, J., and Neira, J. L. (2010) The basic helix-loop-helix region of human neurogenin 1 is a monomeric natively unfolded protein which forms a "fuzzy" complex upon DNA binding. *Biochemistry 49*, 1577–1589.
48. Marsh, J. A., Singh, V. K., Jia, Z., and Forman-Kay, J. D. (2006) Sensitivity of secondary structure propensities to sequence differences between α- and γ-synuclein: Implications for fibrillation. *Protein Sci. 15*, 2795–2804.
49. Dyson, H. J., and Wright, P. E. (2001) Nuclear magnetic resonance methods for elucidation of structure and dynamics in disordered states. *Methods Enzymol. 339*, 258–270.
50. Dyson, H. J., and Wright, P. E. (2004) Unfolded proteins and protein folding studied by NMR. *Chem. Rev. 104*, 3607–3622.
51. Bai, Y., Chung, J., Dyson, H. J., and Wright, P. E. (2001) Structural and dynamic characterization of an unfolded state of poplar apoplastocyanin formed under nondenaturing conditions. *Protein Sci. 10*, 1056–1066.
52. Banci, L., Bertini, I., Boca, M., Calderone, V., Cantini, F., Girotto, S., and Vieru, M. (2009) Structural and dynamic aspects related to oligomerization of apo SOD1 and its mutants. *Proc. Natl. Acad. Sci. U.S.A. 106*, 6980–6985.
53. Nordlund, A., Leinartaite, L., Saraboji, K., Aisenbrey, C., Gröbner, G., Zetterström, P., Danielsson, J., Logan, D. T., and Oliveberg, M. (2009) Functional features cause misfolding of the ALS-provoking enzyme SOD1. *Proc. Natl. Acad. Sci. U.S.A. 106*, 9667–9672.
54. Song, J., Jamin, N., Gilquin, B., Vita, C., and Menez, A. (1999) A gradual disruption of tight side-chain packing: 2D ^{1}H-NMR characterization of acid-induced unfolding of CHABII. *Nat. Struct. Biol. 6*, 129–134.
55. Wei, Z., and Song, J. (2005) Molecular mechanism underlying the thermal stability and pH-Induced unfolding of CHABII. *J. Mol. Biol. 348*, 205–218.
56. Kuwajima, K., Yamaya, H., and Sugai, S. (1996) The burst-phase intermediate in the refolding of β-lactoglobulin studied by stopped flow circular dichroism and absorption spectroscopy. *J. Mol. Biol. 264*, 806–822.

57. Hamada, D., Segawa, S. I., and Goto, Y. (1996) Non-native α-helical intermediate in the refolding of β-lactoglobulin, a predominantly β-sheet protein. *Nat. Struct. Biol. 3*, 868–873.
58. Kuwata, K., Shastry, R., Cheng, H., Hoshino, M., Batt, C. A., Goto, Y., and Roder, H. (2001) Structural and kinetic characterization of early folding events in β-lactoglobulin. *Nat. Struct. Biol. 8*, 151–155.
59. Chikenji, G., and Kikuchi, M. (2000) What is the role of non-native intermediates of β-lactoglobulin in protein folding? *Proc. Natl. Acad. Sci. U.S.A. 97*, 14273–14277.
60. Song, J., Bai, P., Luo, L., and Peng, Z. Y. (1998) Contribution of individual residues to formation of the native-like tertiary topology in the α-lactalbumin molten globule. *J. Mol. Biol. 280*, 167–174.
61. Shaveta, G., Shi, J., Chow, V. T., and Song, J. (2010) Structural characterization reveals that viperin is a radical S-adenosyl-L-methionine (SAM) enzyme. *Biochem. Biophys. Res. Commun. 391*, 1390–1395.
62. Chiti, F., and Dobson, C. M. (2006) Protein misfolding, functional amyloid, and human disease. *Annu. Rev. Biochem. 75*, 333–366.
63. Ross, C. A., and Poirier, M. A. (2004) Protein aggregation and neurodegenerative disease. *Nat. Med. Suppl.,* S10–S17.
64. Liu, J., Zhu, W., Qin, H., and Song, J. (2009) NMR studies reveal a novel mode for hFADD to bind with the unstructured hRTN3 which initiates the ER-stress activated apoptosis. *Biochem. Biophys. Res. Commun. 383*, 433–439.
65. Rane, N. S., Kang, S.-W., Chakrabarti, O., Feigenbaum, L., and Hegde, R. S. (2008) Reduced translocation of nascent prio protein during ER stress contributes to neurodegeneration. *Dev. Cell 15*, 359–370.